

A direct measurement of the electron density turbulence parameter C_1 towards the magnetar XTE J1810-197

VISWESHWAR RAM MARTHI ¹ AND YOGESH MAAN ¹

¹*National Centre for Radio Astrophysics
Tata Institute of Fundamental Research
Post Bag 3, Ganeshkhind, Pune - 411 007, INDIA*

ABSTRACT

We report the first, direct measurement of the electron density turbulence parameter C_1 , enabled by 550-750 MHz observations with the upgraded Giant Metrewave Radio Telescope. The parameter C_1 depends on the power law index of the wavenumber spectrum of electron density inhomogeneities in the ionized interstellar medium. Radio waves propagating through the inhomogeneous ionized medium suffer multipath propagation, as a result of which the pulsed emission from a neutron star undergoes scatter broadening. Consequently, interference between the delayed copies of the scatter-broadened electric field manifests as scintillation. We measure a scintillation bandwidth $\Delta\nu_d = 149 \pm 3$ Hz as well as a scatter-broadening timescale $\tau_d = 1.22 \pm 0.09$ ms at 650 MHz towards the magnetar XTE J1810-197, using which we estimate $C_1 = 1.14 \pm 0.09$ directly from the uncertainty relation. This is the first time that $\Delta\nu_d$ and τ_d have been measured simultaneously at the same frequency, and also the first reported direct measurement of a scintillation bandwidth of order 100 Hz. We describe the methods employed to obtain these results and discuss their implications in general, as well as for the magnetar XTE J1810-197. We also discuss how such, effectively in-situ, measurements of C_1 can aid in inferring the wavenumber spectrum power law index and hence quantitatively discriminate between the various possible scattering scenarios in the ionized medium.

Keywords: Radio transient sources (2008) — Interstellar medium (847) — Interstellar scintillation (855)

1. INTRODUCTION

Pulsars with low dispersion measure (DM) are observed to scintillate at radio frequencies. Scintillation arises from the interference of distorted wavefronts arriving at the observer as a result of multipath propagation through the ionized interstellar medium (IISM). Scintillation is typically observed as bright and faint patterns in the dynamic spectrum. One way to interpret the preponderance of scintillation in low-DM pulsars is the small net cross-section for encountering scattering screens, as low-DM pulsars tend to be nearby ones: fewer screens are likely to be aligned favourably along the line-of-sight (LoS) such that the chance coincidence for destruction of coherence by successive screens is low. It is more likely for phase coherence to be destroyed when a large number of screens are encountered, even if only a fraction of which are favourably aligned: the result is a lack of visible scintles. For example, the nearby pulsar B1133+16 is now known to have at least six scat-

tering screens (McKee et al. 2022) that cause independent scintillation. Stock & van Kerkwijk (2024) note the presence of multiple screens within and near the edge of the Local Bubble, which may be important for scintillation in many low-DM, relatively nearby pulsars. In contrast, pulsars with higher DM, and hence at larger distances, appear to lack prominent scintles in their dynamic spectra. This is understood to be a limitation primarily arising from their small scintillation bandwidths ($\Delta\nu_d$) and limited spectral resolution available to resolve the scintles. However, it is unclear if improving the instrument spectral resolution alone could lead to discerning the scintles clearly in the dynamic spectrum, as the per-pixel signal-to-noise ratio (S/N) would have to be $\gg 1$. This is usually achieved by binning in time and frequency when the scintles are well-resolved, but would become blended in the small $\Delta\nu_d$ regime, precluding such binning along the frequency dimension. Clearly, observing bright pulsars is an implicit prerequisite for resolving small- $\Delta\nu_d$ scintles if detection is to be possi-

ble without spectral binning. Alternatively, a multitude of scattering screens as would be the case for high-DM pulsars, hence more distant, increases the probability for destruction of phase coherence resulting in lack of scintillation. Partial destruction of coherence has been argued even for as few as two screens in B1508+55 by Marthi et al. (2021).

The small $\Delta\nu_d$ is understood to be a direct consequence of large scatter broadening time (τ_d), due to the uncertainty relation (Cordes & Rickett 1998) (hereafter CR98),

$$2\pi\Delta\nu_d\tau_d = C_1 \quad (1)$$

where C_1 is a constant determined by the wavenumber spectrum of the scattering material. The correlation between τ_d and DM is empirically well-established (e.g. Mitra & Ramachandran 2001; Bhat et al. 2004). This means that, often for moderate to high-DM pulsars with appreciable τ_d , $\Delta\nu_d$ is almost never measured directly; it is rather inferred with the aid of the uncertainty relation assuming a specific turbulence power spectrum (and hence C_1), often letting $C_1=1$. Even for low-DM pulsars with negligible scatter broadening and striking scintillation patterns, allowing $\Delta\nu_d$ to be robustly measured, observing with high spectral resolution can lead to interesting discoveries, such as with PSR B0834+06. The high spectral resolution VLBI observations and measurements reported by Brisken et al. (2010) led to the detection of a hitherto unknown second screen and associated exotic optical phenomena such as double lensing (Liu et al. 2016; Zhu et al. 2023). The 1-ms island, arising from refraction off the second screen, would not have been detected if not for the high delays probed in the secondary spectrum, aided of course by the baseband data acquired for VLBI correlations.

For those pulsars that show appreciable τ_d but measuring $\Delta\nu_d$ is challenging, a direct measurement of both the quantities together could be attempted with Nyquist-resolution baseband data. Of course, the ability to measure both the quantities robustly depends on many aspects, e.g., an intelligent choice of the observing frequency (which determines $\Delta\nu_d$), the S/N of the observed pulsed signal and the DM (which may affect τ_d). However, simultaneous measurement of both τ_d and $\Delta\nu_d$ can result in a direct, in-situ estimation of the parameter C_1 . A direct estimate of C_1 can reveal the nature of the scattering material, as C_1 encodes the index β of the wavenumber spectrum through the structure function index γ . In this work, we present our attempt to make an in-situ measurement of C_1 towards a particular source — magnetar XTE J1810-197, which is currently active at radio frequencies. In addition to measuring C_1 , this work is also motivated by the lack of any direct mea-

surement of scintillation bandwidth towards this magnetar so far. Furthermore, intriguing spectral structures in the single pulses from this magnetar have been observed earlier (Maan et al. 2019). The origin of these spectral structures seemed likely to be intrinsic rather than scintillation, and a direct measurement of the scintillation bandwidth could potentially strengthen this deduction.

In the following sections, first we provide the relevant background information and further motivation for this work to be conducted on the particular target (Section 2) followed by details of the observing setup and data analysis (Section 3). We outline our results in Section 4, discuss their implications in Section 5, and summarize the conclusions in Section 6. Throughout this paper, we follow the convention $\Delta\nu_d \propto \nu^\alpha$ and $\tau_d \propto \nu^{-\alpha}$, where α is a positive real number.

2. MAGNETAR XTE J1810-197

The magnetar XTE J1810-197 ($18^{\text{h}}09^{\text{m}}51^{\text{s}}.09$, $-19^{\circ}43'51.93''$) was discovered in X-ray (Ibrahim et al. 2004), with the distinction that it is the first transient Anomalous X-ray Pulsar (AXP). Subsequently, it was detected in radio (Camilo et al. 2006) and observed to have highly variable radio pulsations at the same period as in X-ray, i.e., 5.54 s, and a remarkably flat radio spectrum $S \propto \nu^{-0.5}$ (Camilo et al. 2007a). Although strong and variable pulsations were seen in early observations, it was observed that the average pulse flux density was decreasing with time (Camilo et al. 2007b) and eventually the magnetar became radio quiescent abruptly (Camilo et al. 2016). However, it has recently undergone an outburst in radio with a considerable increase in its average flux density (Lyne et al. 2018; Maan et al. 2019) at the outburst, followed by a secular decrease for many weeks. Additionally, more recent studies report a steeper and variable spectrum (see Maan et al. 2022 for details) after the late-2018 outburst. The source continues to be active, and hence, it is still an opportune time to study this intriguing magnetar in detail.

Magnetar XTE J1810-197 has a DM of 178 pc cm^{-3} . To the best of our knowledge, there are no direct measurements of the scintillation bandwidth and timescale for this source. Maan et al. (2019) report spectral characteristics that resemble interstellar scintillation, but find that the characteristic bandwidths (visually, $\sim 20 - 40 \text{ MHz}$) of these spectral features are inconsistent with the expected scintillation bandwidth derived from the NE2001 model, and hence conclude the features are likely intrinsic. Maan et al. (2019) also report a $\tau_d \sim 1.05 - 1.3 \text{ ms}$ (τ_{sc} in their notation) at 650 MHz, which translates into a small $\Delta\nu_d \sim 140 - 175 \text{ Hz}$ — the only, indirect, measurement of $\Delta\nu_d$ for this source. More

recently, we have also measured a scattering timescale (unpublished) $\tau_d \sim 6$ ms at 400 MHz. Using a scaling index of $\alpha \sim 4$ for the frequency dependence, the expected scatter broadening at 650 MHz would then be $\tau_d \sim 0.86$ ms. This translates roughly into a $\Delta\nu_d \sim 200$ Hz (using $2\pi\Delta\nu_d\tau_d = C_1$, and $C_1 = 1.16$; Cordes & Lazio 2002; Cordes et al. 2004) at 650 MHz, i.e., consistent with the estimates from Maan et al. (2019).

Following the formulation in Lorimer & Kramer (2005), Lazaridis et al. (2008) make an estimate of $\Delta\nu_d \sim 320$ MHz and a scintillation timescale of 10 min at 15 GHz. Extrapolated with $\alpha \sim 4$ to 650 MHz, the expected $\Delta\nu_d \sim 1.2$ kHz. This is $\sim 6 - 10\times$ larger compared to the expectation from the τ_d measurement. However, this estimate could be off by a large amount and, additionally, a small deviation in α could easily explain the discrepancy between the two $\Delta\nu_d$ values. Nevertheless, it remains to be seen if there is a second screen which, e.g., could have caused the spectral structures with typical bandwidths of 20-30 MHz reported by Maan et al. (2019). Moreover, measuring $\Delta\nu_d$ at 650 MHz also holds the potential for a direct, in-situ measurement of C_1 aided by the existing or simultaneous measurements of the scatter broadening time τ_d .

3. OBSERVATIONS AND DATA ANALYSIS

3.1. Baseband voltage beamformer

XTE J1810-197 is being regularly monitored through an independent observing program. However, its scintillation bandwidth and timescale have never been directly measured. The scatter broadening timescale τ_d reported by Maan et al. (2019) as well as unreported measurements at 400 MHz hint at the possibility of extremely small scintillation bandwidths $\lesssim 1$ kHz (at 1 GHz), requiring high-resolution spectroscopy. The phased array beamformer of the GMRT Wideband Backend (GWB) is limited by the GPU FLOPS and other bandwidth constraints to a maximum of 16384 channels. In principle, high spectral resolution can therefore be achieved by trading off observing bandwidth for band-integrated sensitivity.

The ideal observing strategy would be to obtain baseband voltage data, so that near-arbitrary temporal and spectral resolution can be achieved. A newly-unlocked baseband beamformer mode in the GWB, primarily intended for VLBI observations, has therefore been used for the observations reported here. In the Total Intensity mode of the GWB, the beamformed complex voltage spectra are tapped from the output of the GWB F-engine and sent downstream for detection and integration after channelization using the fast fourier transform (FFT). In the newly enabled Phased Array Spectral

Voltage (PASV) mode, the Nyquist-sampled data from the individual polarizations are recorded as complex spectra, i.e. the phased-array FFT output of the beamformer is collected from the ring-buffer shared memory and written to non-volatile memory (NVM) disks, ensuring that the full 200/400 MHz of the baseband is captured without buffer loss.

3.2. Observing setup

XTE J1810-197 was observed with the upgraded GMRT (uGMRT; Gupta et al. 2017) using the time awarded through a Director’s Discretionary Time (DDT) proposal. Observations were conducted in three sessions over a total time of 4 hours. There were two single-band, one-hour observing sessions, one each at Band-4 (550-750 MHz) and Band-5 (1060-1260 MHz). In addition there was a two-hour long, Band-4/5 simultaneous dual-band observation with 100 MHz bandwidth in each band. We recorded a single 200 MHz PASV beam for the single band observations and 2×100 MHz PASV beams for the dual-band observations with two disjoint sub-arrays comprising of different GMRT dishes. The spectrometer was configured with the default settings, giving 2048 channels across 100/200 MHz. The PASV is a complex filterbank format, but it comes with associated header and timestamp files.

3.3. Pre-processing

The PASV filterbank data were first translated to DADA format and then converted to standard coherently dedispersed `sigproc` filterbank using `digifil`. For obtaining the dedispersed time sequence, the filterbank files were produced with 2048 channels with the best fit DM of $178.85 \text{ pc cm}^{-3}$. The time sequence was searched for bright single pulses using PRESTO (Ransom 2001). The detected pulses were then sorted in descending peak flux order and the brightest 20 pulses were considered for further analysis. Their peak-referred time of arrival (ToA) was used to identify the appropriate time segment in the PASV data. Short time segments, typically ± 2.5 s around the peak of the pulse, were then extracted from the PASV data, translated to DADA and `sigproc` filterbank with extremely high spectral resolution.

The Band-4, 200 MHz data were channelized into 2097152 (2M) channels, giving a spectral resolution of ~ 95 Hz per channel. This is required for resolving the putative scintillation if it is expected to be smaller than 1 kHz. For the Band-5 100 MHz data, the number of channels was set to 524288 (0.5M) resulting in spectral resolution half of that in Band-4. However, we use only the Band-4 data for our sensitive measurements as the

Band-5 data turned out to be heavily contaminated by radio frequency interference (RFI) in the middle of the observing band. We therefore discuss the Band-5 data no further.

3.4. Autocorrelation of single-pulse spectra

The spectrum of each of the the identified pulses was obtained by integrating under the ON-gate¹ after weighting by the frequency-averaged profile. The spectrum thus obtained is subdivided into M fine subbands, each consisting of N channels. The autocorrelation function (ACF) is now calculated for each subband for $N - 1$ frequency lags. The ACFs of the 20 identified pulses were stacked and averaged. For Band-4, $M = 1024$ and $N = 2048$. Finally, the 1024 subbands in Band-4 are grouped into 7 coarse subbands of equal frequency widths, after omitting the first and the last 64 fine subbands. Each coarse subband is thus 25-MHz wide. The final, frequency-resolved, ACF obtained is shown in Figure 1.

3.5. Single pulse analysis for scatter broadening

Every pulse emitted by the source undergoes a series of convolutions with multiple different response functions due to the propagation effects of the interstellar medium as well as the electrical response of the instrument. Broadly,

$$S(t, \nu) = P(t, \nu) * G(t, \nu) * D(t, \nu) * I(t, \nu) \quad (2)$$

where S is the observed pulse signal, P is the intrinsic pulse function, G is the interstellar Green's function causing the scatter broadening, D is the dispersion smear function and I is the instrument response function (Ramachandran et al. 1997). Since the data were coherently dedispersed, the dispersion smear function D is effectively a Dirac delta function; I is a *sinc* function whose characteristic width is an inverse function of the frequency resolution set at the time of the observation.

We assume a gaussian for the intrinsic pulse shape and consider a one-sided decaying exponential for the pulse broadening function (PBF). In order to estimate the scatter broadening time, it is essential to identify bright, sharply peaked pulses with a simple morphology or isolated pulse components that can be fit with a single gaussian convolved with a decaying exponential. Pulses with complex morphologies require more gaussian components, resulting in typically poor fits with

large off-diagonal covariance values. In the case of XTE J1810-197, such as is the case for magnetars in general, a complex and unstable pulse profile evolution precludes easy identification of such sharply peaked single-component pulses. A thorough visual search resulted in one such reasonably bright pulse which, however, is not part of the main component. The baseband data segment for this pulselet was extracted from the larger file (as described earlier) and rechannelized to 256 channels to obtain a finer time resolution (163.84 μ s) than that obtained for the scintillation analysis.

4. RESULTS

4.1. Scintillation bandwidth

We fit the ACF of each coarse subband in Figure 1 with a decaying exponential $Ae^{-\Delta\nu/\Delta\nu_d}$, excluding the zero-lag point, to estimate the scintillation bandwidth $\Delta\nu_d$. The intervals between the isoclines are seen to increase with the subband frequency, as expected for scintillation. The fit parameters are listed in Table 1. The values returned by the fit at the coarse subbands show the expected power-law scaling behaviour with frequency. The measured values for $\Delta\nu_d$ are then fit with a power law $\nu_d(\nu) = C_0(\nu/\nu_0)^\alpha$, where $\nu_0=650$ MHz. The fit returned $C_0 = 149.5 \pm 3.3$ Hz and an index of $\alpha = 4.0 \pm 0.3$, which is also broadly consistent with $\alpha = 4.4$ expected for Kolomogorov turbulence. This is likely the first direct measurement of the scintillation bandwidth, in contrast to a scintillation bandwidth inferred from the scatter broadening time, for cases where only the latter is practically measurable. This allows us to independently confirm if the scatter broadening and scintillation arise from the same locales in the interstellar medium. In other words, independent measurements like these are necessary to investigate if the bulk of the scatter broadening arises from the local environs of the pulsar (magnetar in this case) while scintillation could be attributed to one or more intervening screens. Often, for lack of an independent measurement, the inferred scintillation bandwidth (through the uncertainty relation) is attributed to the scatter broadening.

4.2. Scatter broadening time

Figure 2 shows the isolated pulselet used for fitting the scatter broadening time. We fit a gaussian pulse convolved with a decaying exponential (which is the PBF) to the data,

$$s(t) = \frac{S}{\sigma_g \sqrt{2\pi}} e^{-\frac{1}{2} \left(\frac{t-t_0}{\sigma_g} \right)^2} * \frac{1}{\tau_d} e^{-\frac{t}{\tau_d}} \quad (3)$$

where t_0 is the instant at which the gaussian peaks, σ_g is the standard deviation and S is the fluence of the

¹ The ON-gate for each pulse was visually identified due to the complex morphology, but could be defined as the contiguous signal between the extremal points of the pulse roughly above 3.5σ of the root mean square off-pulse noise.

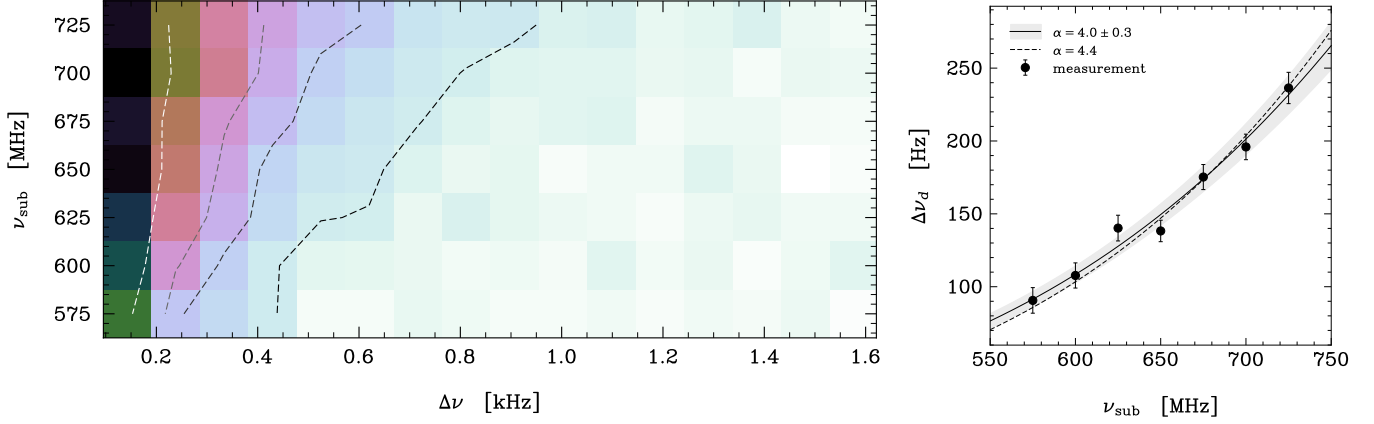


Figure 1. *Left:* The subband-binned autocorrelation function stacked for 20 pulses vs frequency lag. *Right:* The measured $\Delta\nu_d$ values at each subband, along with the error bars and the fits.

Frequency MHz	A	$\Delta\nu_d$ Hz
575	1.45 ± 0.18	90.6 ± 8.8
600	1.47 ± 0.13	107.7 ± 8.6
625	1.23 ± 0.08	140.2 ± 8.8
650	1.54 ± 0.08	138.3 ± 7.4
675	1.24 ± 0.06	175.3 ± 8.6
700	1.30 ± 0.05	195.9 ± 8.8
725	1.07 ± 0.04	236.4 ± 11.7

Table 1. The measured parameters of the one-sided exponential that fit the autocorrelation function giving the $\Delta\nu_d$ values for each subband and the respective error bars.

scatter-broadened pulse. The measured scatter broadening time at 650 MHz is $\tau_d = 1.22^{+0.10}_{-0.09}$ ms which scales to 217^{+18}_{-16} μ s at 1 GHz for $\alpha = 4.0$. The inverse of the spectral channel width makes an additional contribution to the scatter broadening time through a *sinc* function, which we ignore as it is ~ 1.3 μ s for 256 channels across 200 MHz. Effectively, we approximate the *sinc* function as a δ -function for $I(t, \nu)$ in equation 2 and it is small enough to be subsumed under the estimated $\pm 8\%$ error.

5. DISCUSSION

5.1. Scintillation

The detectability of scintillation declines with increasing DM, assuming that the locales where scintillation arise are the same as those responsible for the scatter-broadening, i.e., they arise from the same “screen”. This is largely true, except in those cases where the scatter-broadening may result from a dynamically active region closer to the source, whereas the scintillation may arise in a second screen: if the screen closer to the observer still “sees” an unresolved source despite scatter-broadening, it would cause scintillation independent of the scattering screen. This phenomenon is seen, e.g.,

in the Crab pulsar (Main et al. 2018), where the nebula produces the scatter broadening and an intervening screen in the ISM causes the scintillation. This seems to be somewhat more common in fast radio bursts, although not surprisingly, where the scatter broadening typically arises in the host galaxy whereas the Galactic ISM “sees” an essentially unresolved source (see Masui et al. 2015; Main et al. 2022; Marthi et al. 2022; Sammons et al. 2023, for examples).

Lazaridis et al. (2008) note that at the frequency of their observations, i.e., at 14 GHz, the flux density variations are expected to be large, attributable to scintillation. They argue that the large observing bandwidths and long integration times would average many scintles, thereby yielding reliable flux density estimates. They consider a critical frequency $\nu_c = 14.6$ GHz, above which scintillation is thought to transition from strong to weak. This ν_c is an estimate based on earlier measurements (Malofeev et al. 1996) and the NE2001 electron density model (Cordes & Lazio 2002). They therefore estimate, using expressions given in Lorimer & Kramer (2005), a diffractive scintillation bandwidth $\Delta\nu_d = 320$ MHz and a diffractive scintillation timescale $t_d = 600$ s.

The fit to the measurements (see Figure 1) returns $\Delta\nu_d(650 \text{ MHz}) = 149 \pm 3$ Hz and $\alpha = 4.0 \pm 0.3$, which is also consistent to within 2.5% with a forced Kolmogorov $\alpha = 4.4$ that has been locally fit through the measurements. The shaded region is the $\pm 1\sigma$ error bar for the fit obtained by formally propagating the errors on the α and the $\Delta\nu_d$ measurements. Our $\Delta\nu_d$ measurement at 650 MHz, when extrapolated to 14 GHz is ~ 32 MHz, an order of magnitude smaller.

Maan et al. (2019) detected spectral features which, being inconsistent with the scintillation bandwidth estimated from Cordes & Lazio (2002) as well as that deduced from their own scatter-broadening measurements, they concluded as not arising due to scintillation. Our

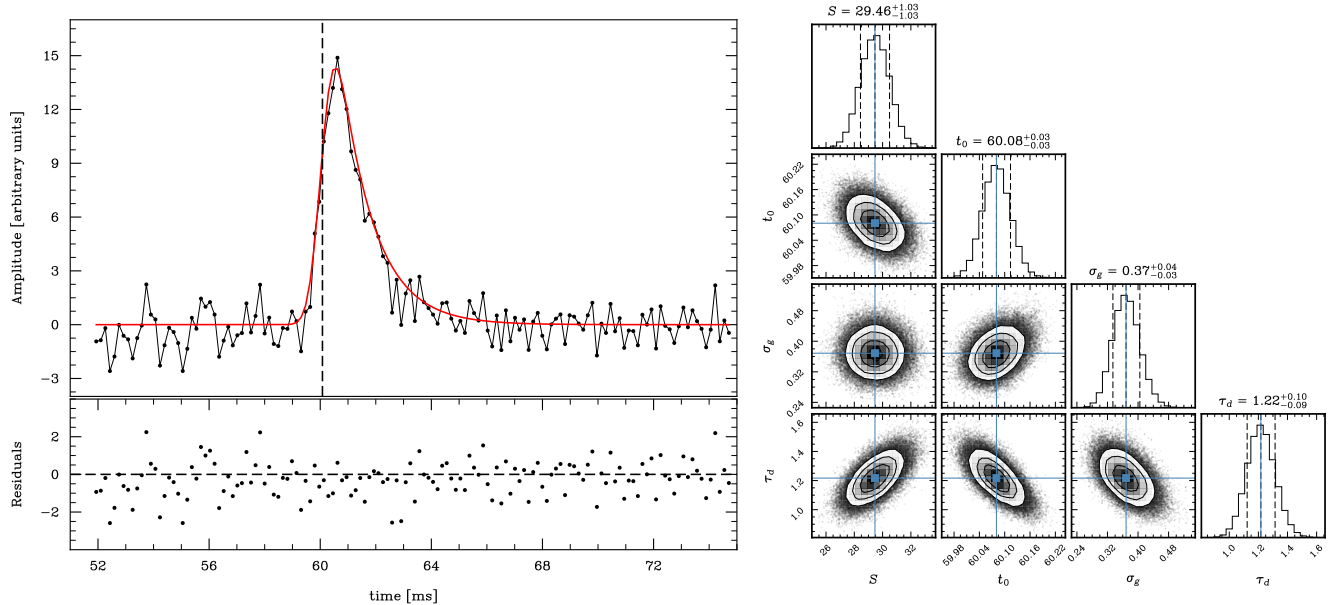


Figure 2. *Left:* The isolated pulselet used for estimating τ_d , along with the fit and the residuals. A decaying exponential with a scale constant τ_d is convolved with a gaussian pulse of width t_w to determine the best fit parameters. *Right:* Corner plots show the excellent constraints obtained on τ_d , which is mildly degenerate with σ_g .

direct measurements of the scintillation bandwidth also support the above conclusion. Furthermore, [Gotthelf et al. \(2004\)](#) present X-ray observations that indicate an absence of any plerionic material around XTE J1810-197. Similarly, no HII emission is detected along the LoS to this magnetar. So, there is no observational signature suggesting the presence of an additional screen which could have caused the observed spectral features. Nonetheless, whether these features are intrinsic and linked to the outburst itself or whether linked to an influence of the outburst on the propagation in the vicinity of the magnetar needs further investigation. If the features are phenomenologically linked to the outburst, we would expect them to also fade with time. High cadence monitoring observations after an outburst could help shed some light on the nature and possible origin of the spectral features.

In addition to the scintillation bandwidth $\Delta\nu_d$, we attempted also to measure the scintillation timescale t_d . This was done by picking adjacent pairs of pulses, with one of each pair coming from the selection of the 20 bright pulses, and computing the cross-correlation function in the same way as the auto-correlation function, but no cross-correlation was detected. [Lazaridis et al. \(2008\)](#) estimate a scintillation time $t_d \sim 600$ s at 15 GHz, which scales to 26 s at 650 MHz. The Galactic Electron Density model NE2001 ([Cordes & Lazio 2002](#)) predicts $t_d \sim 12.5$ s for this line of sight for $DM=178.85$ pc cm^{-3} at 1 GHz, which translates to 6.9 s to 9.4 s in the GMRT Band-4. The complete absence of cross-correlation be-

tween adjacent pulse pairs in Band-4 suggests a scintillation timescale $t_d < P_0$.

5.2. Scatter broadening

Figure 2 (right) shows the posterior distribution of the maximum-likelihood estimates of the parameters S , t_0 , σ_g and τ_d , obtained through a Markov Chain Monte Carlo (MCMC) simulation. The best fit model and the residuals are shown in the left panel. We note that, and not surprisingly, that σ_g and τ_d are a mildly degenerate pair. S is uncorrelated with σ_g since it merely scales the normalized gaussian. Ideally, we would expect S to be uncorrelated with τ_d , but note that there is a S/τ_d in equation 3 that could explain the partial correlation.

The τ_d measured is the characteristic time of a decaying exponential, with which a gaussian is convolved: while we have used τ_d in the uncertainty relation given by equation 1, the more appropriate quantity to use is the mean delay time τ_{delay} (see eqn. 8 of CR98). For a thin screen ($\Delta s/s \ll 0.01$), $\tau_{\text{delay}} = \tau_d$, since the scattered pulse can be considered the result of a convolution of the intrinsic pulse with a single decaying exponential. For a thick screen, the mean delay time τ_{delay} is not the same as the scatter broadening time τ_d , and cannot be measured unambiguously. CR98 define τ_d as an infinite sum of decay times τ_{d_n} , where each contribution comes from an infinitesimally thin screen. Since recursive convolution of decaying exponentials eventually produces a gaussian, it is possible to arrange for a large number of screens such that the dominant screen

makes the largest contribution to scatter broadening, while the gaussian “intrinsic pulse” is degenerate with multiple sub-dominant instances of scatter broadening. The measured τ_d is hence the most dominant contribution to the effect.

We consider only the simplest PBF, which is the decaying exponential. We have a single scatter-broadened pulselet in our data to deduce the decay time. In principle, we could fit other PBFs, such as those listed in [Bhat et al. \(2004\)](#), [Lambert & Rickett \(1999\)](#) and [Cordes & Lazio \(2002\)](#). Integrated pulse profiles, typically obtained for pulsars, would allow for better discrimination between such candidate PBFs due to the superior S/N. An unstable and very wide (compared to the scatter broadening) pulse profile precludes such analysis robustly for the magnetar.

5.3. C_1

The combination of τ_d and $\Delta\nu_d$ measurements, obtained from the fits at the centre of the band, 650 MHz, effectively translates to a measurement of C_1 , giving $C_1 = 1.14 \pm 0.09$, where the $1\text{-}\sigma$ error bar is computed from the respective errors in fits to the measurements of $\Delta\nu_d$ and τ_d . We denote the structure function index by γ to avoid confusion with the power law index for frequency scaling α (which is the structure function index in the notation of CR98). Our estimate of C_1 is perfectly consistent with a uniform medium with Kolmogorov wavenumber spectrum ($\gamma = 5/3$, $C_1 = 1.16$). However, it is also in agreement with a thin screen with structure function index $\gamma = 2$ ($C_1 = 1$) at 1.5σ , as well as a thin screen with a structure function index $\gamma = 5/3$ (i.e. Kolmogorov; $C_1 = 0.957$), at 2σ . Our measurement rules out a Kolmogorov screen with a square law structure function ($\gamma = 2$, $C_1 = 1.53$) at $> 4\sigma$.

5.4. Implications for the scattering medium

The index α is determined by the wavenumber spectrum in the medium through a power law (with index β ; e.g. [Rickett 1977](#), [Krishnakumar et al. 2015](#)) of the power spectrum of the electron density fluctuations. Being a LoS-integrated measure, local conditions along the LoS cannot be inferred. [Bhat et al. \(2004\)](#) note that departure from the frequency scaling index $\alpha = 4.4$ is possible when there is an inner-scale cut-off in the wavenumber, or an intrinsically non-Kolmogorov wavenumber spectrum. The third effect they consider is bulk refraction that could bias the scatter broadening time upward. However, $C_1 \sim 1$ rules out the particular two-screen model where the scatter-broadened magnetar appears unresolved to a foreground screen.

Figure 3 shows the Galactic NE2001 model ([Cordes & Lazio 2002](#)) radial electron density profile for the slice

through $gb = -0.158^\circ$ for $0^\circ < gl \leq 360^\circ$, indicating no significant density enhancement along the direction of the magnetar out to a distance of 3.5 kpc. However, due to its negative latitude, the LoS to the magnetar from Earth (which is ~ 30 pc above the Galactic plane) encounters a significant amount of material in the plane. The empirical DM– τ_d relation along with the $\pm 1\sigma$ error is shown in the right panel. The black points indicate pulsars > 2.5 kpc around a 10° radius of the magnetar for which τ_d is measured. A few pulsars show significant departure above 1σ , but this is not entirely unexpected — these could be reconciled by invoking a shallow index for α for particular lines of sight, e.g., as a result of upscattering due to bulk refraction.

The observations reported here cannot discriminate reliably between the two possibilities, namely between an inner-scale cutoff and non-Kolmogorov spectrum, for the line of sight to XTE J1810-197. The error bars on the measured $\Delta\nu_d$ and τ_d are limited by (a) the inability to utilise the full exposure on the magnetar to estimate $\Delta\nu_d$, as only the brightest 20 pulses were considered due to the unstable pulse morphology and (b) estimating τ_d from a single pulselet due to the complex, multi-component profile. A similar analysis may be attempted for a sample of bright pulsars where it may be possible to measure both $\Delta\nu_d$ from the full scintillation dynamic spectrum and τ_d from the PBF much more reliably, gaining from the stable folded profile. In fact, millisecond pulsars with measurable scatter broadening time of $\tau_d \sim 1$ ms can serve as excellent probes, for which one can also measure $\Delta\nu_d$ as described above. Measured over multiple independent sightlines to different millisecond pulsars with a range of DMs, one might be able to get more accurate estimates of C_1 across a subset of the observable (DM, τ_d) parameter space.

6. SUMMARY

Magnetar XTE J1810-197 is among the handful that continues to be active in radio frequencies, well past its last outburst in X-ray and hence being continually monitored for spectral and flux evolution ([Maan et al. 2019](#)). Although some spectral features resembling scintillation were observed, these have been concluded to have been intrinsic, as the measured characteristic spectral widths are not commensurate with the scatter broadening times. Our $\Delta\nu_d$ measurement from this work further strengthens the above conclusion. Though, it is not yet clear if these features were related to the 2018 outburst.

We have reported the first ever direct measurement of the scintillation bandwidth $\Delta\nu_d$ for this magnetar at any frequency, and simultaneously with τ_d . We stack the autocorrelation function of the brightest pulses to esti-

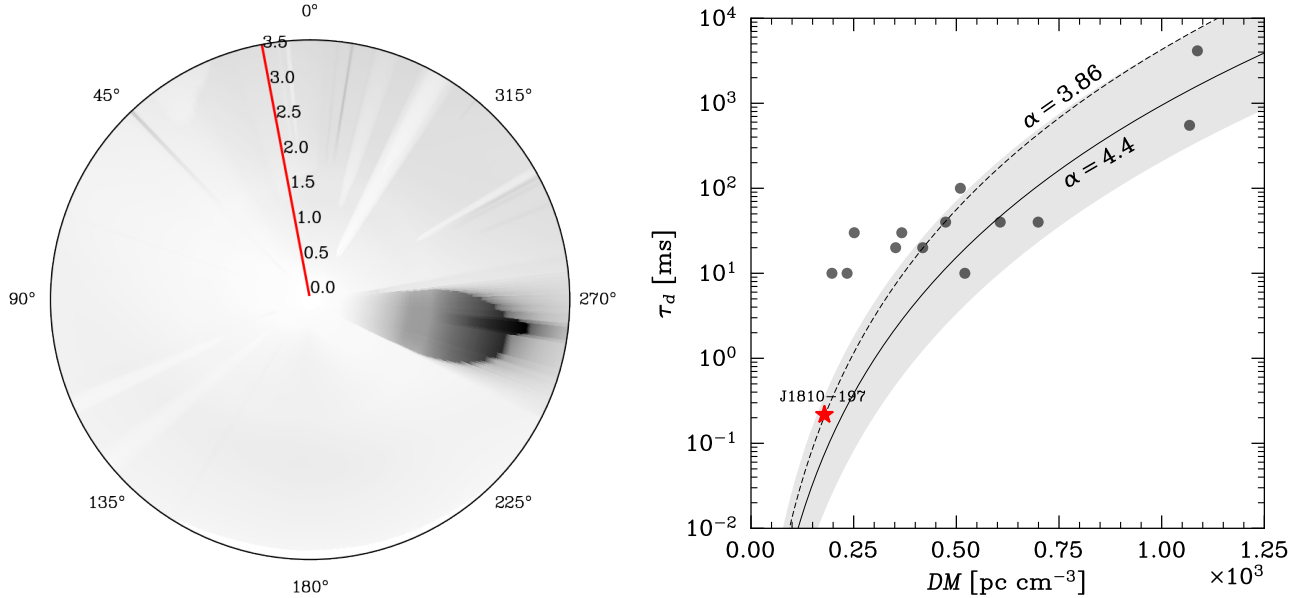


Figure 3. *Left:* The electron density model for $gb = -0.158^\circ$, the Galactic latitude of J1810-197, out to a distance of 3.6 kpc from Earth. The red marker line is in the direction of the magnetar. *Right:* The DM- τ_d of Bhat et al. (2004) is represented by the dashed line; the solid line and the shaded region represent the empirical fit and the error bar σ_{τ_d} with $\alpha = 4.4$ obtained from Cordes & Lazio (2003), all at 1 GHz. The points represent pulsars within 10° of XTE J1810-197 beyond 2.5 kpc.

mate $\Delta\nu_d = 149 \pm 3$ Hz at 650 MHz. Along with $\tau_d = 1.22 \pm 0.09$ ms, these measurements enable us to directly infer $C_1 = 1.14 \pm 0.09$, which depends on the power-law index β of the electron density wavenumber spectrum and hence the index α of the frequency dependence of the scatter broadening timescale τ_d . While our measurement of C_1 rules out a two-screen model, it is unable to robustly discriminate between Kolmogorov ($\gamma = 5/3$), as well as between a uniform scattering medium and a thin screen. A uniform scattering medium with a square law phase structure function is also ruled out at 4σ . The extended IISM can be represented as a succession of randomly oriented, infinitesimally thin screens, such that the screen with the most dominant contribution to the scatter broadening leads to the measured τ_d , while the multitude of subdominant screens convolve out an arbitrary intrinsic pulse function to a gaussian.

Following the successful demonstration of the feasibility of making direct measurements of C_1 in this work, we propose systematic, baseband observations of moderate- and high-DM pulsars along different sightlines to build a sample of the LoS IISM out to different DMs and distances. Empirical estimation of C_1 along multiple sightlines will aid in refining the electron density tomograph of the Milky Way.

7. ACKNOWLEDGEMENTS

YM acknowledges support from the Department of Science and Technology via the Science and Engineering Research Board Startup Research Grant (SRG/2023/002657). We gratefully acknowledge the Department of Atomic Energy, Government of India, for its assistance under project No. 12-R&D-TFR-5.02-0700. We thank the staff of GMRT who made these observations possible. GMRT is run by the National Centre for Radio Astrophysics of the Tata Institute of Fundamental Research. Some computations were performed on the Niagara supercomputer at the SciNet HPC Consortium. SciNet is funded by Innovation, Science and Economic Development Canada; the Digital Research Alliance of Canada; the Ontario Research Fund: Research Excellence; and the University of Toronto.

Facilities: Giant Metrewave Radio Telescope (GMRT)

Software: `dspsr` (van Straten & Bailes 2011), `RFIClean` (Maan et al. 2021), `NumPy` (Harris et al. 2020), `astropy` (Astropy Collaboration et al. 2022), `matplotlib` (Hunter 2007), `splotlib` (Li 2023), `statsmodels` (Seabold & Perktold 2010), `emcee` (Foreman-Mackey et al. 2013), `corner` (Foreman-Mackey 2016).

REFERENCES

- Astropy Collaboration, Price-Whelan, A. M., Lim, P. L., et al. 2022, *ApJ*, 935, 167, doi: [10.3847/1538-4357/ac7c74](https://doi.org/10.3847/1538-4357/ac7c74)
- Bhat, N. D. R., Cordes, J. M., Camilo, F., Nice, D. J., & Lorimer, D. R. 2004, *ApJ*, 605, 759, doi: [10.1086/382680](https://doi.org/10.1086/382680)
- Brisken, W. F., Macquart, J. P., Gao, J. J., et al. 2010, *ApJ*, 708, 232, doi: [10.1088/0004-637X/708/1/232](https://doi.org/10.1088/0004-637X/708/1/232)
- Camilo, F., Ransom, S. M., Halpern, J. P., et al. 2006, *Nature*, 442, 892, doi: [10.1038/nature04986](https://doi.org/10.1038/nature04986)
- Camilo, F., Ransom, S. M., Peñalver, J., et al. 2007a, *ApJ*, 669, 561, doi: [10.1086/521548](https://doi.org/10.1086/521548)
- Camilo, F., Cognard, I., Ransom, S. M., et al. 2007b, *ApJ*, 663, 497, doi: [10.1086/518226](https://doi.org/10.1086/518226)
- Camilo, F., Ransom, S. M., Halpern, J. P., et al. 2016, *ApJ*, 820, 110, doi: [10.3847/0004-637X/820/2/110](https://doi.org/10.3847/0004-637X/820/2/110)
- Cordes, J. M., Bhat, N. D. R., Hankins, T. H., McLaughlin, M. A., & Kern, J. 2004, *ApJ*, 612, 375, doi: [10.1086/422495](https://doi.org/10.1086/422495)
- Cordes, J. M., & Lazio, T. J. W. 2002, doi: [10.48550/ARXIV.ASTRO-PH/0207156](https://doi.org/10.48550/ARXIV.ASTRO-PH/0207156)
- Cordes, J. M., & Lazio, T. J. W. 2003, arXiv e-prints, astro, doi: [10.48550/arXiv.astro-ph/0301598](https://doi.org/10.48550/arXiv.astro-ph/0301598)
- Cordes, J. M., & Rickett, B. J. 1998, *The Astrophysical Journal*, 507, 846, doi: [10.1086/306358](https://doi.org/10.1086/306358)
- Foreman-Mackey, D. 2016, *The Journal of Open Source Software*, 1, 24, doi: [10.21105/joss.00024](https://doi.org/10.21105/joss.00024)
- Foreman-Mackey, D., Hogg, D. W., Lang, D., & Goodman, J. 2013, *PASP*, 125, 306, doi: [10.1086/670067](https://doi.org/10.1086/670067)
- Gotthelf, E. V., Halpern, J. P., Buxton, M., & Bailyn, C. 2004, *ApJ*, 605, 368, doi: [10.1086/382232](https://doi.org/10.1086/382232)
- Gupta, Y., Ajithkumar, B., Kale, H. S., et al. 2017, *Current Science*, 113, 707, doi: [10.18520/cs/v113/i04/707-714](https://doi.org/10.18520/cs/v113/i04/707-714)
- Harris, C. R., Millman, K. J., van der Walt, S. J., et al. 2020, *Nature*, 585, 357, doi: [10.1038/s41586-020-2649-2](https://doi.org/10.1038/s41586-020-2649-2)
- Hunter, J. D. 2007, *Computing in Science & Engineering*, 9, 90, doi: [10.1109/MCSE.2007.55](https://doi.org/10.1109/MCSE.2007.55)
- Ibrahim, A. I., Markwardt, C. B., Swank, J. H., et al. 2004, *ApJL*, 609, L21, doi: [10.1086/422636](https://doi.org/10.1086/422636)
- Krishnakumar, M. A., Mitra, D., Naidu, A., Joshi, B. C., & Manoharan, P. K. 2015, *ApJ*, 804, 23, doi: [10.1088/0004-637X/804/1/23](https://doi.org/10.1088/0004-637X/804/1/23)
- Lambert, H. C., & Rickett, B. J. 1999, *ApJ*, 517, 299, doi: [10.1086/307181](https://doi.org/10.1086/307181)
- Lazaridis, K., Jessner, A., Kramer, M., et al. 2008, *MNRAS*, 390, 839, doi: [10.1111/j.1365-2966.2008.13794.x](https://doi.org/10.1111/j.1365-2966.2008.13794.x)
- Li, J. 2023, *AstroJacobLi/smplotlib: v0.0.6, v0.0.6*, Zenodo, doi: [10.5281/zenodo.7839250](https://doi.org/10.5281/zenodo.7839250)
- Liu, S., Pen, U.-L., Macquart, J. P., Brisken, W., & Deller, A. 2016, *MNRAS*, 458, 1289, doi: [10.1093/mnras/stw314](https://doi.org/10.1093/mnras/stw314)
- Lorimer, D. R., & Kramer, M. 2005, *Handbook of Pulsar Astronomy*
- Lyne, A., Levin, L., Stappers, B., et al. 2018, *The Astronomer's Telegram*, 12284, 1
- Maan, Y., Joshi, B. C., Surnis, M. P., Bagchi, M., & Manoharan, P. K. 2019, *ApJL*, 882, L9, doi: [10.3847/2041-8213/ab3a47](https://doi.org/10.3847/2041-8213/ab3a47)
- Maan, Y., Surnis, M. P., Chandra Joshi, B., & Bagchi, M. 2022, *ApJ*, 931, 67, doi: [10.3847/1538-4357/ac68f1](https://doi.org/10.3847/1538-4357/ac68f1)
- Maan, Y., van Leeuwen, J., & Vohl, D. 2021, *A&A*, 650, A80, doi: [10.1051/0004-6361/202040164](https://doi.org/10.1051/0004-6361/202040164)
- Main, R., Yang, I. S., Chan, V., et al. 2018, *Nature*, 557, 522, doi: [10.1038/s41586-018-0133-z](https://doi.org/10.1038/s41586-018-0133-z)
- Main, R. A., Hilmarsson, G. H., Marthi, V. R., et al. 2022, *MNRAS*, 509, 3172, doi: [10.1093/mnras/stab3218](https://doi.org/10.1093/mnras/stab3218)
- Malofeev, V. M., Shishov, V. I., Sieber, W., et al. 1996, *A&A*, 308, 180
- Marthi, V. R., Simard, D., Main, R. A., et al. 2021, *MNRAS*, 506, 5160, doi: [10.1093/mnras/stab1970](https://doi.org/10.1093/mnras/stab1970)
- Marthi, V. R., Bethapudi, S., Main, R. A., et al. 2022, *MNRAS*, 509, 2209, doi: [10.1093/mnras/stab3067](https://doi.org/10.1093/mnras/stab3067)
- Masui, K., Lin, H.-H., Sievers, J., et al. 2015, *Nature*, 528, 523, doi: [10.1038/nature15769](https://doi.org/10.1038/nature15769)
- McKee, J. W., Zhu, H., Stinebring, D. R., & Cordes, J. M. 2022, *ApJ*, 927, 99, doi: [10.3847/1538-4357/ac460b](https://doi.org/10.3847/1538-4357/ac460b)
- Mitra, D., & Ramachandran, R. 2001, *A&A*, 370, 586, doi: [10.1051/0004-6361:20010274](https://doi.org/10.1051/0004-6361:20010274)
- Ramachandran, R., Mitra, D., Deshpande, A. A., McConnell, D. M., & Abies, J. G. 1997, *Monthly Notices of the Royal Astronomical Society*, 290, 260, doi: [10.1093/mnras/290.2.260](https://doi.org/10.1093/mnras/290.2.260)
- Ransom, S. M. 2001, PhD thesis, Harvard University, Massachusetts
- Rickett, B. J. 1977, *ARA&A*, 15, 479, doi: [10.1146/annurev.aa.15.090177.002403](https://doi.org/10.1146/annurev.aa.15.090177.002403)
- Sammons, M. W., Deller, A. T., Glowacki, M., et al. 2023, *MNRAS*, 525, 5653, doi: [10.1093/mnras/stad2631](https://doi.org/10.1093/mnras/stad2631)
- Seabold, S., & Perktold, J. 2010, in *9th Python in Science Conference*
- Stock, A. M., & van Kerkwijk, M. H. 2024, arXiv e-prints, arXiv:2407.16876, doi: [10.48550/arXiv.2407.16876](https://doi.org/10.48550/arXiv.2407.16876)
- van Straten, W., & Bailes, M. 2011, *PASA*, 28, 1, doi: [10.1071/AS10021](https://doi.org/10.1071/AS10021)
- Zhu, H., Baker, D., Pen, U.-L., Stinebring, D. R., & van Kerkwijk, M. H. 2023, *ApJ*, 950, 109, doi: [10.3847/1538-4357/acdcde0](https://doi.org/10.3847/1538-4357/acdcde0)